Solar Energy 180 (2019) 360–371

Contents lists available at ScienceDirect

Solar Energy

journal homepage: www.elsevier.com/locate/solener

Thermal and thermo-hydraulic analysis of arc shaped rib roughened solar air heater integrated with fins and baffles

P.T. Saravanakumar[a], D. Somasundaram[b,*], M.M. Matheswaran[b]

[a] Department of Mechanical Engineering, KPR Institute of Engineering and Technology, Coimbatore, Tamil Nadu 641407, India
[b] Department of Mechanical Engineering, Jansons Institute of Technology, Coimbatore, Tamil Nadu 641659, India

ARTICLE INFO

Keywords:
Solar air heater
Fins
Baffles
Artificial roughness
Effective efficiency

ABSTRACT

Present study deals with thermo hydraulic performance enhancement of solar air heater (SAH) with various design configurations. Analytical modeling is carried out to study the effect of absorber plate integrated with arc shaped rib roughened barrier with fins and baffles on thermal and effective efficiency of SAH. Variations of flow factors such as Reynolds number and temperature rise parameter with reference to baffle design parameters are presented. The proposed SAH improves the energy and effective efficiency by 28.3% and 27.1% compared with arc shape rib roughened solar air heater. From the results, it is also concluded that lower baffle width and length values provide maximum effective efficiency at higher mass flow rates. Further, the correlations as a function of Reynolds number, baffle width, length and number of fins is developed for predicting the values of effective efficiency. Thereafter, a plot is developed for comparing analytical effective efficiency with predicted effective efficiency and it is found that the averaged deviation of 13%. This present mathematical model for proposed SAH is validated with models available in the literature.

1. Introduction

As per the Paris agreement, it is reported that the global average temperature rise is about 2 °C and concentration of CO_2 is 400 ppm. As energy sectors could be decarbonized to avoid the disastrous climate impact, the 100% renewable energy concepts are discussed among climate scientists and energy experts who expected to achieve this target by 2050. As per the Global Status Report 2016 (GSR, 2016), energy used for heating is about 40% of the total world final energy demand. Therefore, the future of the heating sector requires more research on renewable heating technologies. One of the significant systems for heating is solar air heater (SAH) among the various energy conversion systems. SAH is a simple device used for converting incident solar energy into thermal energy that can be used in process heating applications such as industrial, agricultural, space heating. For enhancing the performance of the SAH, the convective heat transfer coefficient between air and absorber plate is improved by various techniques such as flowing the fluid on both side of absorber plate, impinging jet heat transfer, recycling of air, attaching fins with baffles, artificial roughness and packed beds.

Effect of geometry and operating parameters on thermal and effective efficiency is investigated in order to attain the optimum performance of SAH. For various Reynolds number, the effect of grit geometry is analyzed by (Karmare and Tikekar, 2007) and found that roughness parameter of 1.72 gives maximum performance. Bhushan and Singh (2012) developed the mathematical model for evaluating the thermo hydraulic performance of SAH with protrusion roughness. In this work, the design plots are developed for finding the optimum values of roughness geometric parameters. Similarly, Karwa and Chauhan (2009) carried out an analytical work for evaluating the thermo hydraulic performance discrete V down rib roughened SAH. It is found that at optimum design conditions, the mass flow rate up to 0.04 Kg/s performs better when compared with smooth SAH. Providing arc shaped wire ribs in S shape, SAH of having aspect ratio 12 performs better than SAH with smooth duct (Kumar et al., 2017). From the experimental study (Varun et al., 2008; Yadav et al., 2013) it is found that heat transfer is enhanced for both inclined and transverse rib attached with absorber plate. Later experiment reveals that the enhancements in maximum heat transfer and friction factor are 2.89 times and 2.93 times better as compared with smooth SAH. It is evident that the thermal efficiency and effective efficiency of SAH with arc shaped rib roughened SAH are better than those with other shapes of obstacles (Sahu and Prasad, 2017). From a mathematical model developed by Matheswaran et al. (2018), the single pass double duct SAH with arc shaped roughness reduces CO_2 mitigation by 2.11 times per year and increases the revenue of carbon credit by 2.85 times.

* Corresponding author.
E-mail address: soms.iitm@gmail.com (D. Somasundaram).

https://doi.org/10.1016/j.solener.2019.01.036
Received 29 October 2018; Received in revised form 18 December 2018; Accepted 11 January 2019

Nomenclature

A_{Pl}	area of absorber plate (m^2)
A_{baff}	area of baffle (m^2)
A_{fin}	area of fin (m^2)
AR	arc shaped roughness
C_p	specific heat of air (J/kg K)
D_h	hydraulic diameter of air flow path (m)
e/D_h	rib height-to-duct hydraulic diameter ratio
f_r	friction factor of duct
g	acceleration due to gravity (m^2/s)
h_c	convective heat transfer coefficient (W/m^2 K)
h_r	radiative heat transfer coefficient (W/m^2 K)
h_{wd}	convective heat transfer coefficient due to wind, (W/m^2 K)
h_{nc}	natural convective heat transfer coefficient between glass and absorber plate (W/m^2 K)
L	length of the duct (m)
$\dot{m}_a$	mass flow rate of air (kg/s)
Nu	Nusselt number
N_O	number of fins
P_{me}	pumping power (W)
q_u	useful heat gain (W)
Re	Reynolds number
S	intensity of solar radiation (W/m^2)
M_1 to M_{10}	factors used in matrices
T	temperature (K)
U_{be}	bottom loss coefficient (W/m^2 K)
V_{wd}	wind velocity (m/s)
W	width of the collector (m)
W_B	width of the baffle (m)
L_B	length of the baffle (m)
Z_2	height of the duct (m)
h_f	height of the fin (m)
t_{fin}	thickness of the fin (m)
k_{fin}	thermal conductivity of the fin
τ	transmissivity of glass cover
μ_a	viscosity (kg/m s)
ϕ_x	dimension less parameter
ρ_a	density (kg/m^3)
σ	Stefan's Boltzmann constant ($W/m^2 K^4$)
η_I	thermal efficiency (%)
η_{eff}	effective (or) thermo hydraulic efficiency
η_{fin}	fin efficiency
η_{baff}	baffle efficiency
θ	tilt angle (°)
ΔP_a	pressure drop (N/m^2)
ε	emissivity
α	absorptivity
k_a	thermal conductivity (W/m K)

Subscripts

am	ambient air
be	back plate
gc	glass cover
ai	inlet
in	insulation
a	air in the channel
ao	outlet
pl	absorber plate
sy	sky

Further, the enhancement of thermal performance of SAH with extended surfaces attached with absorber plate is investigated. Experimentations on SAH with array of rectangular fins arranged longitudinally is conducted (Fakoor Pakdaman et al., 2011). In this study, the effect of the solar radiation and ambient temperature on thermal efficiency is analyzed using order of magnitude analysis. It is concluded that the effect of solar radiation is 79 times better than that of ambient temperature. Fudholi et al. (2013) presented the experimental and analytical results of double pass SAH with and without fins. It is observed that the thermal efficiency is proportional to solar intensity at particular mass flow rate. With fins, the thermal efficiency is enhanced by 9% due to increase in convection heat transfer coefficient. Based on benefit cost ratio, it is concluded that the double pass SAH with fins are cost effective. Ammari (2003) carried out analytical study to investigate the performance of the solar air heater with slat and found that the influence of geometrical parameters on the first law efficiency. He concluded that the slat thickness variation is less significant compared to the distance between glass cover and absorber plate. Further the effect of rectangular fin on thermal efficiency is investigated and found that fins with thin metal sheet SAH performs better up to the *Re* = 22,000 (Bahrehmand et al., 2015). Singh and Dhiman (2015), developed mathematical model and CFD simulation to investigate the effect of rectangular fins with semicircular duct. From the CFD results, it is reported that the SAH with more fins performs better due to more heat transfer area. Priyam and Chand (2016, 2018) developed a theoretical model for investigating the performance of wavy finned SAH. They concluded that the wave length, amplitude and fin spacing could affect the performance of SAH. With less fin spacing, the effective efficiency is enhanced by 35.6% at lower mass flow rate. In addition, amplitude with 2.5 cm and wave length of 3 cm provides the maximum thermal and effective efficiency.

Kumar and Chand (2017, 2018) conducted analytical study of SAH with herringbone corrugated fins. It is found that effect of fin pitch and fin spacing ratio on thermal and effective efficiency are significant and its values are 66.9% at mass flow rate of 0.033 kg/s and 68.9% for the mass flow rate of 0.05 kg/s. They also used twisted tape to enhance the thermal and effective efficiency. Using MATLAB codes, most efficient operation of SAH attached with fins is found out at twist ratio of 2. SAH with offset fins are used for increasing the thermal and effective efficiency by 74.5%, 72.5% at lower mass flow rate (Rai et al., 2017, 2018). Using louvered fins of various spacing, the thermal efficiency is enhanced from 43.1% to 72.5% at fixed mass flow rate then decreasing the effective efficiency by 9.4% is observed due to increase in pressure drop (Chand and Chand, 2018). Chamoli and Thakur (2016) developed a correlation for Nusselt number and friction factor for SAH with V down perforated baffles. From the experimental results it is found that the maximum heat transfer is attained for the relative roughness ranging from 1.5 to 3.

Thermal performance of SAH with upward type baffles is studied by Yeh et al. (2000). It is found that thermal efficiency of SAH with fins and baffles are higher than that of SAH with fins and conventional parallel pass SAH. Mohammadi and Sabzpooshani (2013, 2014) analytically investigated the effect of fins and baffles on thermal performance of SAH at steady state conditions. Effect of geometry parameters of baffles and number of fins are subjected to variations for evaluation of thermal and effective efficiency. It is evident that for fixed length of the baffle, increasing the width increases the thermal and effective efficiency. However, for fixed width of baffle, increasing the length of the baffles leads to decrease in both efficiencies. Further investigation reveals that recycling with above same configuration boost up the energy efficiency. However, at high mass flow rate, the decline in effective efficiency is observed.

With reference to above discussion on thermal performance enhancement methods of SAH, It is evident that the many researchers

focused on SAH with artificial roughness or fins or fins with baffles. It is also known that the artificial roughness used for breaking the laminar sub layer formulation, fins and baffles used for improving the flow behavior are separately available in the literature.

Therefore, the present works deals with enhancing the thermal performance of SAH by integrating fins with baffles attached with arc shaped rib roughened absorber plate. Detailed theoretical investigation for proposed SAH is to be developed by mass and energy balance equations. Using MATLAB code, the effect of geometry and operating parameters on thermal performance of SAH will be investigated. Further, the correlation will be developed for predicting the effective efficiency as a function of design and operating parameters such as baffle length, width, number of fins and Reynolds number.

2. Mathematical modeling of proposed solar air heater

The proposed cross-sectional view of SAH, combined with arc shaped rib roughness attached below the absorber plate with fins and baffles, is shown in Fig. 1a. It comprises of transparent glass cover, arc shaped rib roughened absorber plate integrated with fins and baffles placed Z_3 distance away from glass cover, back plate located at Z_2 distance from absorber plate and insulation of thickness Z_1. The glass cover mounted on the top of the SAH reduces the top heat loss to the ambient. The space between the absorber plate and back plate formulates the air flow channel. When the air flows to the channel, it extracts heat from the absorber plate. To improve the rate convective heat transfer between the absorber plate and flowing air, the arc shaped

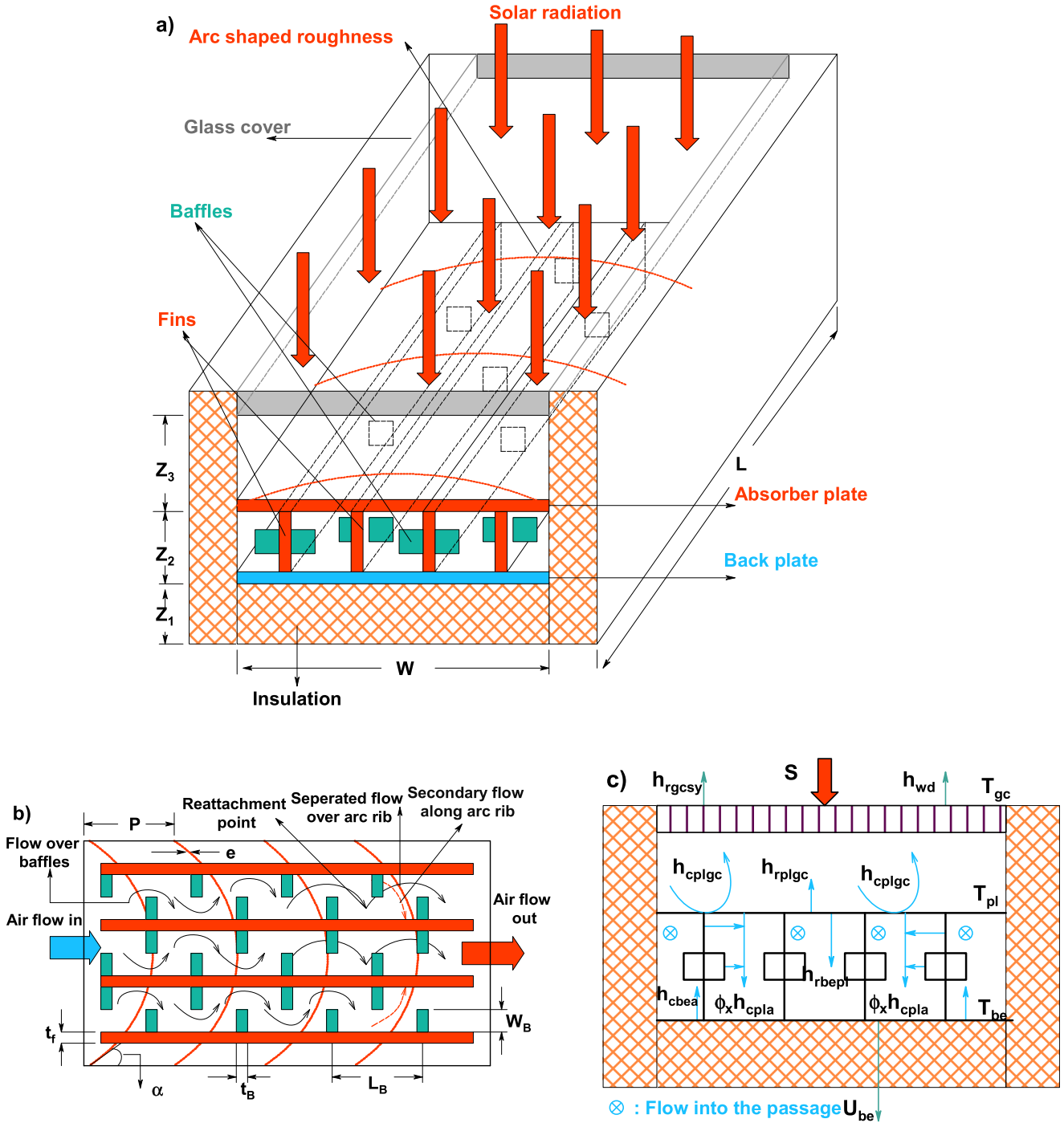

Fig. 1. (a) Cross sectional view of SAH, (b) arrangement of arc shaped ribs, fins with baffles on absorber plate, (c) energy balance at SAH.

rib roughness, fins with baffles are attached at the bottom of the absorber plate as shown in Fig. 1b. The arc shaped ribs breaks the laminar sub layer formulation and generates the secondary flow separations with reattachment points. The fins which enhance the rate of convective heat transfer from absorber plate and the baffles guide the air in the flow path and make it more turbulent.

Fig. 1c represents the terms used to develop the basic energy balance equations governing the heat transfer between the SAH components. Without violating the fundamental physics of heat transfer and to analytically evaluate the system performance, the following assumptions are considered (Matheswaran et al., 2018).

1. Performance of the SAH is evaluated at steady state operating condition and one-dimensional heat transfer analysis along the fluid flow direction is considered.
2. With respect to its position of the SAH, the convective heat transfer coefficient is constant
3. Air flow paths are completely sealed to arrest the leakage of air.
4. Thermal conductivity and heat capacity of glass, absorber plate, fins, baffles and insulation are constant.
5. For longer wave length of solar radiation, the sky is acted as a black body.

3. Energy balance equations for SAH components

The glass cover receives part of energy from solar radiation and the remaining amount of energy from the absorber plate due to the convective and radiative heat transfer. It also liberates the energy to the ambient and sky as considered as top heat loss. The energy balance at glass cover can be written as

$$\alpha_{gc}S + h_{nc}(T_{pl} - T_{gc}) + h_{r,\,pl-gc}(T_{pl} - T_{gc}) = h_{wd}(T_{gc} - T_{am}) + h_{r,\,gc-sy}(T_{gc} - T_{sy}) \quad (1)$$

The absorber plate receives energy from direct solar radiation and it transfers this energy to the glass cover and back plate by convective and radiative heat transfer. It is also transferring the heat to the flowing fluid and it is considered as use full heat gain. The energy balance at absorber plate can be written as

$$\alpha_{pl}\tau_{gc}S = h_{c,pl-gc}(T_{pl} - T_{gc}) + h_{r,pl-gc}(T_{pl} - T_{gc}) + \phi_x\, h_{c,pl-a}(T_{pl} - T_a) + h_{r,pl-be}(T_{pl} - T_{be}) \quad (2)$$

When the air flows through the channel formulated by absorber and back plate of the SAH, it gains thermal energy from both the plates of the air heater. The rate of convective heat transfer is enhanced by attaching the arc shaped ribs, fins with baffles at the bottom of the absorber plate. The energy balance for air flow through the channel is written as

$$q_{u1} = \phi_x\, h_{c,pl-a}(T_{pl} - T_a) + h_{c,be-a}(T_{be} - T_a) \quad (3)$$

In the above Eq. (3) ϕ_x is the dimension less parameter which represents the influence of fins with baffles attached at the bottom of the absorber plate. (Mohammadi and Sabzpooshani, 2013, 2014) and $T_a = (T_{ai} + T_{ao})/2$, $q_{u1} = 2\dot{m}_a C_p (T_a - T_{ai})/WL$ represent the average air temperature and useful energy gain at the air channel.

$$\phi_x = 1 + \frac{A_{fin}}{A_{pl} - A_{b-fin}}\eta_{fin} + \frac{A_{baff}}{A_{pl} - A_{b-fin}}\eta_{baff} \quad (4)$$

From Eq. (4) it is observed that when the SAH is operated without fins and baffles, the second and third terms are cancelled and the value of the $\phi = 1$. By considering the influence of these extended surfaces, the corresponding terms are included in the equation. The efficiency of the fin (η_{fin}) is calculated by using the relation (Mohammadi and Sabzpooshani, 2013, 2014)

$$\eta_{fin} = \frac{\tanh(mh_{fin})}{mh_{fin}} \quad (5)$$

In the above Eq. (5)

$$m = \sqrt{\frac{2(h_{c\,pl-a}(L + t_{fin})}{k_{fin}Lt_{fin}}} \quad (6)$$

The efficiency of the baffles (η_{baff}) can be calculated by using the empirical correlation given by Mohammadi and Sabzpooshani (2013, 2014)

$$\eta_{baff} = 15.583\left[\frac{W_B}{D_h}\right]^{0.0518}\left[\frac{L}{L_B}\right]^{-0.2247} \quad (7)$$

The back plate receives energy from the absorber plate by radiative heat transfer and it transfers this energy to the flowing fluid as use full heat gain and the part of the heat lost to the ambient is considered as bottom loss. The bottom loss of the SAH is minimized by providing the insulation of required thickness. The energy balance for back plate is written as

$$h_{r,pl-be}(T_{pl} - T_{be}) = h_{c,be-a}(T_{be} - T_a) + U_{be}(T_{be} - T_a) \quad (8)$$

3.1. Temperature calculations of SAH components

To evaluate the temperature of various components of SAH, from Eqs. (1)–(3) and (8) it is expressed in matrix form as shown in Eq. (9).

$$\begin{bmatrix} M_5 & M_6 & 0 & 0 \\ M_7 & M_8 & -\phi_x h_{cpla} & -h_{rplbe} \\ 0 & \phi_x h_{cpla} & M_9 & h_{cbea} \\ 0 & h_{rplbe} & h_{cbea} & M_{10} \end{bmatrix}\begin{bmatrix} T_{gc} \\ T_{pl} \\ T_a \\ T_{be} \end{bmatrix} = \begin{bmatrix} M_1 \\ M_2 \\ M_3 \\ M_4 \end{bmatrix} \quad (9)$$

where

$$M_1 = \alpha_{gc}S + h_{wd}T_{am} + h_{r,\,gc-sy}T_{sy} \quad (10)$$

$$M_2 = \alpha_{pl}\tau_{gc}\,S \quad (11)$$

$$M_3 = -(2\,\dot{m}_a\,C_p/WL)T_{ai} \quad (12)$$

$$M_4 = -U_{be}T_a \quad (13)$$

$$M_5 = (h_{wd} + h_{r,\,gc-sy} + h_{r,\,pl-gc} + h_{nc}) \quad (14)$$

$$M_6 = -(h_{c,\,pl-gc} + h_{r,pl-gc}) \quad (15)$$

$$M_7 = -(h_{c,\,pl-gc} + h_{r,pl-gc}) \quad (16)$$

$$M_8 = (h_{c,\,pl-gc} + h_{r,\,pl-gc} + \phi_x\, h_{c,\,pl-a} + h_{r,\,pl-be}) \quad (17)$$

$$M_9 = -\left[\phi_x\, h_{c,pl-f} + h_{c,be-f} + \left[\frac{2\dot{m}C_p}{WL}\right]\right] \quad (18)$$

$$M_{10} = (h_{c,be-a} + U_{be} + h_{r,pl-be}) \quad (19)$$

Eq. (9) is rearranged in the form of $[T] = [M]^{-1}[C]$. Then the temperature of the solar air heater components is calculated by using matrix inversion technique by means of the code generated in MATLAB.

3.2. Thermo physical properties and heat transfer coefficient for simulation

The thermo physical property of air varies linearly with respect to temperature. These values are calculated by using the following relations (Ong, 1995).

$$C_p = 1.0057 + 6.6 \times 10^{-5}(T - 27) \quad (20)$$

$$\rho_a = 1.1774 - 3.59 \times 10^{-3}(T - 27) \quad (21)$$

$$k_a = 0.02624 + 7.58 \times 10^{-5}(T - 27) \quad (22)$$

$$\mu_a = [1.983 + 0.00184(T - 27)] \times 10^{-5} \quad (23)$$

The empirical correlation used to determine the convective heat transfer coefficient between the top glass cover and wind flowing over the glass is given by Matheswaran et al. (2018).

$$h_{wd} = 2.8 + 3.3V_{wd} \quad (24)$$

The relation used to find the radiation heat transfer coefficient between the top glass cover and sky is given by Fudholi et al. (2013)

$$h_{r,gl-sy} = \sigma\varepsilon_{gc}(T_{gc} + T_{sy})(T_{gc}^2 + T_{sy}^2) \quad (25)$$

In the above equation Tsy is the sky temperature and it can be calculated using the following relation (Fudholi et al., 2013)

$$T_{sy} = 0.0552T_a^{1.5} \quad (26)$$

The natural convective heat transfer occurred between the absorber plate and glass cover happens due to trapped air between the components. The heat transfer coefficient between the plate and cover is given by Hollands et al. (1976)

$$h_{nc} = \frac{k_a}{Z_3}Nu_{nc} \quad (27)$$

$$Nu_{nc} = 1 + 1.44\left[1 - \frac{1708(sin1.8\theta)^{1.6}}{Ra\ cos\theta}\right]\left[1 - \frac{1708}{Ra\ cos\theta}\right]^{+} + \left[\left(\frac{Ra\ cos\theta}{5830}\right)^{1/3} - 1\right]^{+} \quad (28)$$

The above equation effectively evaluates the Nusselt number, when the tilt angle (θ) of the SAH is up to 60°. The positive values in the fourth term of Eq. (28) are only to be considered. The Rayleigh number is given by Hollands et al. (1976).

$$Ra = \frac{g\beta(T_{pl} - T_{gc})Z_3}{\alpha_a \nu_a} \quad (29)$$

The relation used to find the radiation heat transfer coefficient between the top glass cover and absorber plate is given by Sahu and Prasad (2017)

$$h_{r,\ pl\ -\ gc} = \frac{\sigma(T_{pl}^2 + T_{gc}^2)(T_{pl} + T_{gc})}{\frac{1}{\varepsilon_{pl}} + \frac{1}{\varepsilon_{gc}} - 1} \quad (30)$$

The forced convective heat transfer occurs between the absorber plate and air flowing through the channel. The heat transfer coefficient between the plate and flowing air is given by

$$h_{c,\ pl\ -\ a} = \frac{k_a}{D_h}Nu_{c,pl\ -\ a} \quad (31)$$

In the above Eq. (31), the Nusselt number ($Nu_{c,pl\ -\ a}$) can be expressed (Sahu and Prasad, 2017) as

$$Nu_{c,pl\ -\ a} = 0.001047Re^{1.3186}\left(\frac{e}{D_h}\right)^{0.3772}\left(\frac{\alpha}{90}\right)^{-0.1198} \quad (32)$$

The hydraulic diameter (D_h) of the air flow channel of the SAH is given by

$$D_h = \frac{4WZ_2}{2(W + Z_2)} \quad (33)$$

When the fins and baffles are attached to the bottom of the absorber plate, then the hydraulic diameter of the SAH is given by

$$D_h = \frac{4(WZ_2 - N_o h_{fin} t_{fin})}{2(W + Z_2) + N_o(h_{fin} + t_{fin})} \quad (34)$$

The relation used to find the radiation heat transfer coefficient between the back plate and absorber plate is given by Matheswaran et al. (2018).

$$h_{r,\ pl\ -\ be} = \frac{\sigma(T_{pl}^2 + T_{be}^2)(T_{pl} + T_{be})}{\frac{1}{\varepsilon_{pl}} + \frac{1}{\varepsilon_{be}} - 1} \quad (35)$$

The forced convective heat transfer occurs between the back plate and air flowing through the channel. The heat transfer coefficient between the back plate and flowing air is given by Fudholi et al. (2013)

$$h_{c,\ be\ -\ a} = \frac{k_a}{D_h}Nu_{c,be\ -\ a} \quad (36)$$

In Eq. (36) the Nusselt number ($Nu_{c,be\ -\ a}$) can be expressed as

$$Nu_{c,be\ -\ a} = 0.116(Re_a^{2/3} - 125)Pr^{1/3} + \left[1 + \left[\frac{Dh}{L}\right]^{\frac{2}{3}}\right]\left[\frac{\mu_a}{\mu_w}\right]^{0.14} \quad (2300 < Re_a < 6000) \quad (37)$$

$$Nu_{c,be\ -\ a} = 0.018Re_a^{0.8}Pr^{0.4} \quad (Re_a > 6000) \quad (38)$$

3.3. Pressure drop and pumping power requirement for SAH channel

The pumping power required to overcome the friction along the length of all the configurations of SAH is calculated by

$$P_{me} = \frac{\dot{m}_a \times (\Delta P_a)}{\rho_a} \quad (39)$$

In the above Eq. (39), the pressure drop (ΔP_a) occurred along the length of arc shape rib roughened SAH is calculated by using the relation

$$\Delta P_a = \frac{2f_r LV^2\rho_a}{D_h} \quad (40)$$

When the pressure drop occurs, the friction factor (f) is calculated using the relation (Sahu and Prasad, 2017).

$$f_r = 0.14408Re_a^{-0.17103}\left(\frac{e}{D_h}\right)^{0.1765}\left(\frac{\alpha}{90}\right)^{0.1185} \quad (41)$$

The pressure drop (ΔP_a) occurred along the length of arc shape rib roughened SAH attached with fins and baffles is calculated by using the relation (Mohammadi and Sabzpooshani, 2013, 2014).

$$\Delta P_a = (1.465 \times 10^{-5})Re_a^{1.94}\left(\frac{W_B}{D_h}\right)^{2.6}\left(\frac{L}{L_B}\right)^{1.2} + \frac{2fLV^2\rho_a}{D_h} \quad (42)$$

3.4. Thermal and effective efficiency of SAH

As per the First Law of Thermodynamics, the fraction of useful energy gained by the working fluid is calculated based on the equation (Duffie and Beckman, 2013)

$$\eta_I = \frac{Q_u}{A_{pl} \times S} = \frac{\dot{m}_a C_{pa}(T_{oa} - T_{ia})}{A_{pl} \times S} \quad (43)$$

The consumption of pump work is also to be considered to evaluate the realistic performance of the solar air heater. Due to the presence of artificial roughness, fins with baffles attached to the absorber plate increase the pressure drop and improve the pumping power consumption. The mechanical pumping power is converted in to thermal energy equivalent by using the conversion factor C_j and the effective efficiency is calculated by using the following relationship (Chauhan and Thakur, 2014)

$$C_j = \eta_{Th}\eta_{fr}\eta_m\eta_f \quad (44)$$

$$\eta_{eff} = \frac{Q_u - \left[\frac{P_{me}}{C_j}\right]}{S \times A_{pl}} \quad (45)$$

The value of C_j is equal to 0.2 and calculated by using various efficiencies such as efficiency of power plant, mechanical transmission efficiency, efficiency of the motor and blower efficiency (Matheswaran et al., 2018).

3.5. Theoretical solution procedure

The solution procedure for solving the energy balance Eqs. (1)–(3) and (8) using the computer developed code in MATLAB is shown in the flow chart (Fig. 2). In this work, matrix inversion technique is used to evaluate the temperatures of various components of the SAH. During initialization, the ambient temperature, thermal properties and design parameters of SAH components, (shown in Table 1) are given as initial inputs. Then the temperature of various components of SAH and air flow mean path temperatures are suitably assumed. Based on this temperature values, the thermo physical properties of air are calculated using Eqs. (20)–(23). Further, the required convective and radiative heat transfer coefficients are evaluated by using the correlations given in Eqs. (5)–(34). By inverting Eq. (9), the required temperatures of the SAH components are evaluated. Then the evaluated temperature values are compared with earlier assumptions and the temperature variations in the range of $\leqslant 0.01\ ^{\circ}C$ is identified when the solution is converged. Further, the temperature values are used to calculate the thermal and effective efficiency of the SAH.

4. Results and discussions

The thermal performance of arc shape rib roughened solar air heater combined with fins and baffles is analytically analyzed based on the fixed and variable design parameters as shown in Table 1. The influences of baffle length and width, mass flow rate and numbers of fins on the thermal and effective efficiency are investigated and its optimum values are reported in the following subsections.

4.1. Validation of the present theoretical model

For validating the numerical procedure and its code, developed in MATLAB, the results are compared with results reported in the literature. Fig. 3 compares the thermal and effective efficiency of the developed model of arc shape wire roughened SAH with previous study by Sahu and Prasad (2017) and have the maximum deviation of 4.7% and 4.3% respectively. Further the analytical model of SAH with fins and the combination of fins and baffles are compared with experimental and analytical work by Karim and Hawlader (2006) and Yeh et al. (2000). The results show that the present work has the average deviation of 5.4% and 4.7% respectively. This ensures the reliability of the present mathematical model for further analysis.

4.2. Effect of fins with baffles attached with artificial roughness on thermal efficiency

Fig. 4 shows the effect of *Re* number on thermal efficiency and outlet temperature for various design configurations of SAH. It reveals the trend that the increasing *Re* number enhances thermal efficiency monotonically and decreases the outlet temperature steeply. It is due to the fact that increasing *Re* number induces turbulence flow and increases heat capacity of the fluid thereby results in increased heat transfer rate. In addition to this, it reduces the outlet temperature of the air due to less contact time between the absorber plate and flowing air. Figure also shows the importance of incorporation of fins on thermal efficiency. Added fins increases the thermal efficiency of SAH by maximum of 7% due to increased surface area for the heat transfer compared with arc shaped rib roughened SAH. Further, the thermal efficiency is drastically increased by attaching the baffles on the fins. As baffles disintegrate and mix the flow of fluid, heat transfer between arc shape rib roughened absorber plates and flowing fluid is maximized.

This figure also illustrates the influence of geometry parameter of the baffle on thermal efficiency and outlet temperature. As the baffle width increases, both the thermal efficiency and outlet temperature also increase while other parameters are constant. It is also seen that the increase in efficiency is more significant for *Re* number up to 8500 and less significant when *Re* increases further. At higher *Re* number, the effect of baffle width on thermal efficiency is not significant due to progression in flow separation. The increase in thermal efficiency of maximum of 22.4%, 26.5% and 28.3% for baffles width of 0.005, 0.01 and 0.015 m are observed when compared with arc shaped rib roughened SAH. From Eq. (8), it is known that the width of baffles can affect the efficiency of the baffle. It is also evident that the dimensionless parameter (ϕ) is function of baffle efficiency. Therefore increase in width of baffle increases baffle efficiency by more flow violation and mixing. Consequently this can improves the heat transfer rate between absorber plate and flowing fluid.

Fig. 5 represents the contribution of length of baffle on thermal efficiency of SAH for arc shaped rib roughened absorber combined with fins and baffles. As baffle efficiency is strong function of length as given in Eq. (8), the small increase in length results in significant increase in thermal efficiency. When the length of baffle is halved, increases in thermal efficiency is of 1% to 8% from higher value of *Re* to lower value. It is due to that fact that, when number of baffles is increased, the length of the baffle is decreased. As a result, more turbulence is created and it induces the flow separation due to arc shaped roughness. Further, the generated secondary flow takes more heat along the arc ribs and it reattaches with primary flow causing of breaking of laminar sub layer formation. Consequence of this phenomenon results in enhancing the heat transfer.

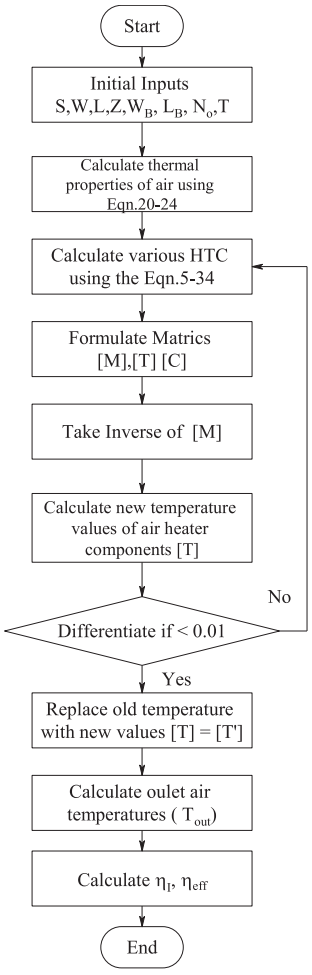

Fig. 2. Flow chart for analytical solution procedure.

Table 1
Typical values of operating and Design parameters used in analytical study.

S. no.	Parameters	Base values
Fixed design and operating parameters		
1	Duct Length, L	1.5 m
2	Duct Width, W	1 m
3	Duct Height, Z_2	0.03 m
4	Air gap between absorber plate and glass cover (d),	0.05 m
5	Thickness of insulation, δ_{in}	0 0.05 m
6	Thermal conductivity of insulation k_i	0.037 W/m K
7	Emissivity of absorber plate,ε_{pl}	0.9
8	Emissivity of bottom plate, ε_{be}	0.9
9	Emissivity of glass cover, ε_{gc}	0.88
10	Effective transmittance absorptance product, $\tau\alpha_{pl}$	0.8
11	Atmospheric temperature, T_a	300 K
12	Wind velocity, V_{wd}	1.5 m/s
13	Rib height-to-duct hydraulic diameter ratio, (e/D_h)	0.0422
14	Flow-attack-angle, $(\alpha/90)$	0.333
15	Relative roughness pitch (P/e)	10
16	Height of the fin (h_f)	0.03 m
17	Thickness of the fin (t_f)	0.001 m
18	Thermal conductivity of the fin (k_{fin})	14.9 W/m K
Variable design and operating parameters		
1	Reynolds Number (Re)	2900–17000
2	Width of the Baffle (W_B)	0.005–0.015 m
3	Length of the Baffle (L_B)	0.2–0.4 m
4	Number of fins (N_O)	2–10
5	Solar Intensity, (S)	800 W/m^2

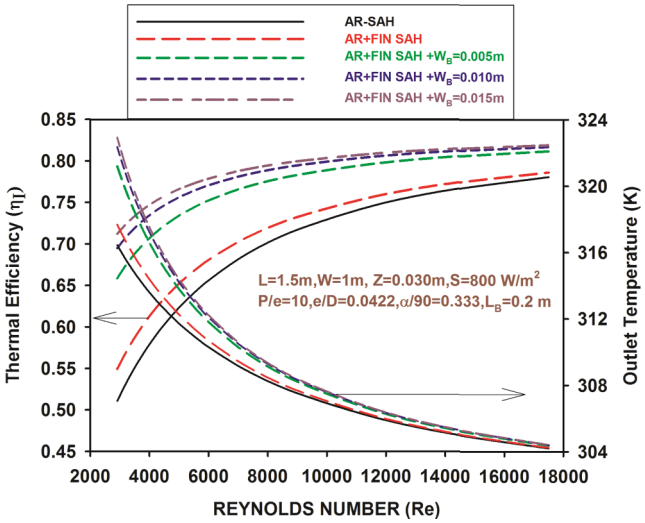

Fig. 4. Effect of Reynolds number on thermal efficiency and *outlet temperature* for various configurations of SAH.

4.3. Effect of fins with baffles attached with artificial roughness on effective efficiency

Figs. 6–8 show the effect of *Re* number on effective efficiency for

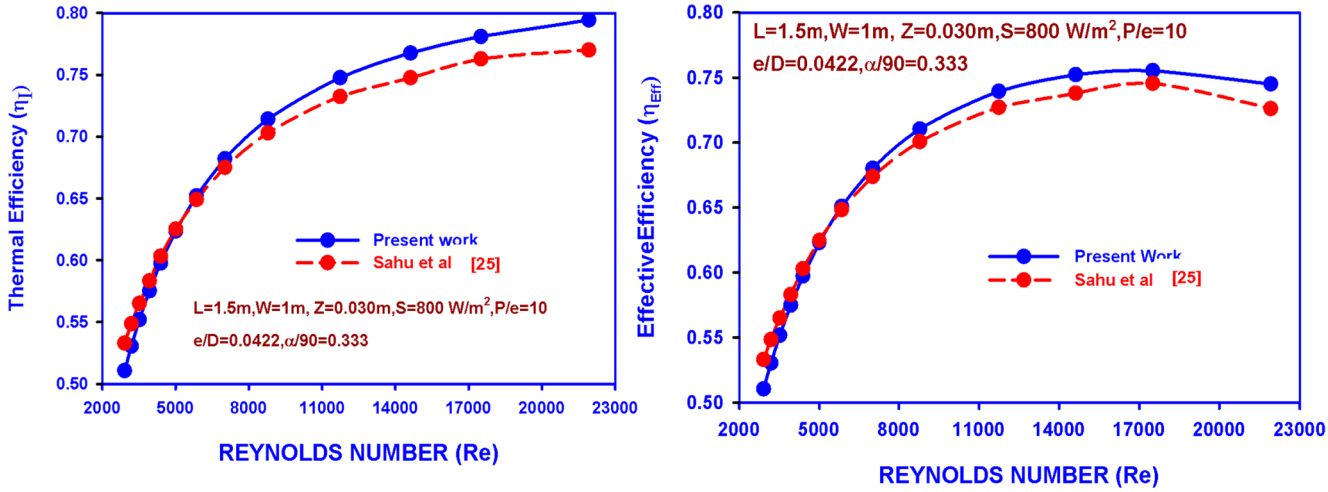

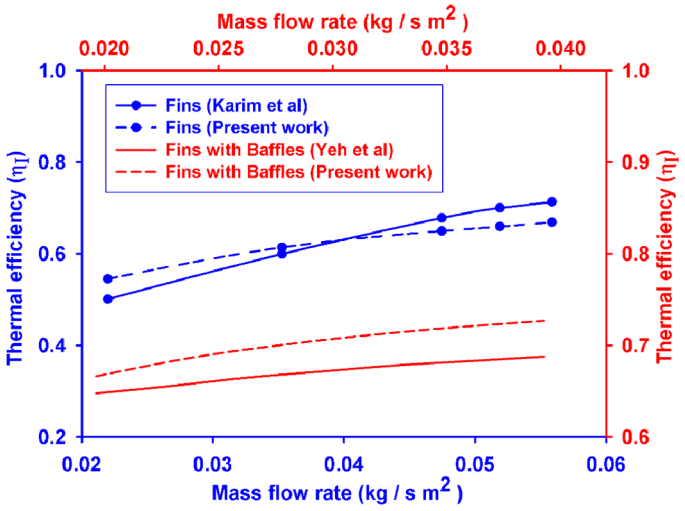

Fig. 3. Validation of present work based on thermal and effective efficiency.

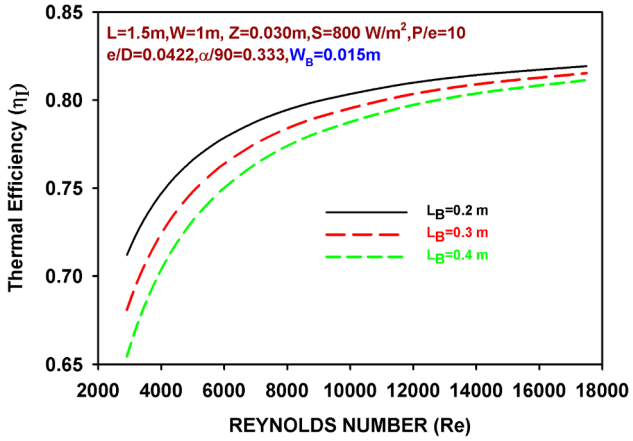

Fig. 5. Effect of Reynolds number and length of the baffles on thermal efficiency of SAH.

various configuration of SAH. Fig. 6 illustrate the significance of width of baffle on effective efficiency at fixed length of baffle while other parameters are constant. From this figure, effective efficiency for AR + FIN SAH is better than that of the AR-SAH and it is about 7% at lower *Re*. Variation in effective efficiency gradually decreases when *Re* increases. At *Re* value of 14,000, the effective efficiency of AR-SAH is more than that of AR + FIN SAH due to higher pressure drop of flowing fluid caused by combined effect of higher mass flow rate and presence of fins. The contribution of effect of baffle width on effective efficiency is also shown in this figure. At low *Re*ynolds number, effective efficiency with baffle width of 0.005, 0.010 and 0.015 m are 22.4%, 26.2% and 27.1% higher than that of AR-SAH.

Even though the contribution of the fins and baffle on thermal efficiency is noticeable, it deteriorates the effective efficiency. For $L_B = 0.2$ m, $W_B = 0.015$ m, the effective efficiency is maximum up to *Re* = 4000. Beyond this values, effective efficiency is maximum for $W_B = 0.010$ m about *Re* value of 6000. When *Re* is greater than 6000 for $W_B = 0.005$ m, the maximum effective efficiency is maintained. Even though high turbulence contributes to higher heat transfer when baffle width increases, it increases the pressure drop of flowing fluid leading to higher pumping power resulting in lower effective efficiency.

The same curve trends are observed when lengths of baffles change as 0.3 m and 0.4 m as shown in Figs. 7 and 8. From Fig. 7, at low Reynolds number, effective efficiency with baffle width of 0.005, 0.010 and 0.015 m are 17.8%, 22.3% and 24.6% higher than that of AR-SAH. For $L_B = 0.3$ m, $W_B = 0.015$ m, the effective efficiency is maximum up to *Re* = 5000. Beyond this values, effective efficiency is maximum for $W_B = 0.010$ m about *Re* value of 7000. When *Re* is greater than 7000 for $W_B = 0.005$ m, the maximum effective efficiency is maintained. As shown in Fig. 8, when *Re* is greater than 7000 for $L_B = 0.4$ m, $W_B = 0.005$ m, the maximum effective efficiency is maintained. At low Reynolds number, effective efficiency with baffle width of 0.005, 0.010 and 0.015 m are 14.8%, 19.1% and 21.6% higher than that of AR-SAH. It is evident from the above discussion that the increase in length of baffles decreases the enhancement of effective efficiency due to lower heat gain even though pumping power is lower.

From the above results and discussions, the maximum efficiency is obtained for the baffles width of 0.005 m. In order to optimize the length of baffle, the analysis is carried out by keeping all other parameters constant as shown in Fig. 9. In this figure, it is observed that the length of the baffle of 0.2 m gives maximum effective efficiency for *Re* up to 12000. When *Re* value is greater than 12000, $L_B = 0.4$ m performs better. It is due to the fact that the number of baffles are more, when SAH operates at *Re* < 12000, $L_B = 0.2$ m. As a result, it increases the heat gain comparatively higher than the value of increment in pumping power.

Figs. 10 and 11 show the relationship between temperature rise parameter and effective efficiency as s function of width and length of the baffle. It is also evidenced that the maximum effective efficiency of 77.3% is obtained for the baffle width and length of 0.005 and 0.2 m. From Fig. 10, it is observed that the effective efficiency first steeply increases and attains maximum and then decreases linearly when the temperature rise parameter increases gradually. When the temperature rise parameter is in the range of 0.004 to 0.013 Km^2/W, the width of baffle of 0.005 m grants the maximum effective efficiency. Further, when it increases from 0.0131 to 0.02 Km^2/W, the maximum effective efficiency is obtained for the width of 0.01 m. Further promoting this temperature rise parameter range, the maximum effective efficiency is obtained for the width of 0.015 m.

It is shown in Fig. 11 that the effective efficiency first steeply raises and reaches maximum and then falls down linearly when the temperature rise parameter increases steadily for the various length of the baffle. When the temperature rise parameter ranges from 0.004 to 0.0064 Km^2/W, the length of baffle of 0.4 m gives the maximum effective efficiency. Further, when it increases from 0.0065 to 0.008 Km^2/W, the maximum effective efficiency is obtained for the length of 0.3 m. Further, promoting this temperature rise parameter results in maximum effective efficiency for the length of 0.2 m. The significance of Figs. 10 and 11 is to select the optimum dimension of the SAH to operate it at desired temperature rise parameter.

4.4. Effect of number of fins on effective efficiency

Fig. 12 illustrates the significant effect of number of fins on effective efficiency. When the *Re* value increases, the effective efficiency rises steeply up to certain value and then starts to decrease due to raise in pumping power. When the number of fins increases, the effective efficiency also shoots up at corresponding *Re* value. When *Re* values are greater than 17,100, 16,190, 15,300, 14,600 and 13,900 for number fins of 2, 4, 6, 8 and 10, the effective efficiency drops down due to higher pressure drop. The maximum enhancement in effective efficiency with respect to arc shaped roughened rib SAH is of 8.5, 14, 17.3, 19.4 and 20.1% for n = 2, 4, 6, 8, and 10 respectively. Increase in effective efficiency is not appreciable after number fins exceed more than 8. Therefore, when n = 8, the optimum performance of SAH is obtained

Fig. 13 shows the effective efficiency as a function of solar radiation for various values of Reynolds number. It is observed that the effective efficiency increases with increase in solar radiation. When the solar

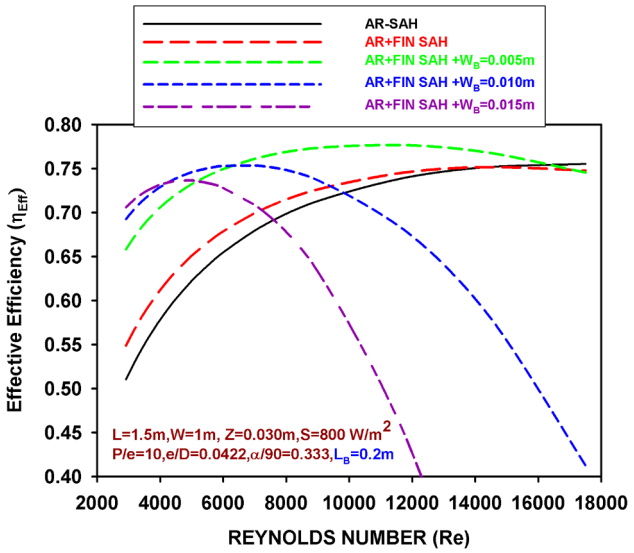

Fig. 6. Effect of Reynolds number and width of the baffle on effective efficiency of SAH when $L_B = 0.2$ m.

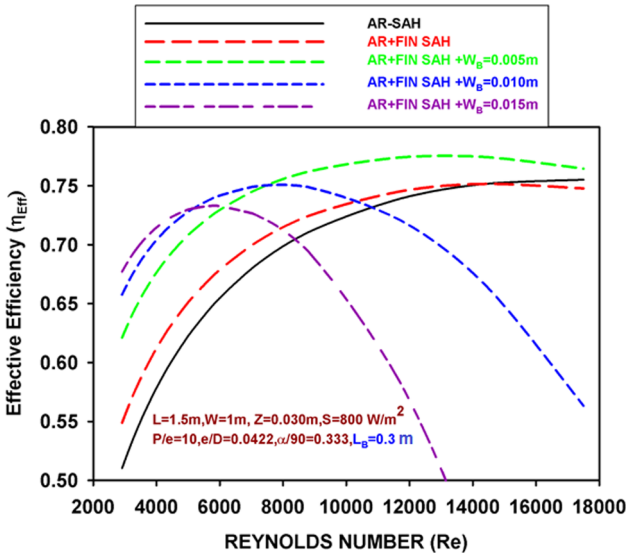

Fig. 7. Effect of Reynolds number and width of the baffle on effective efficiency of SAH when L_B = 0.3 m.

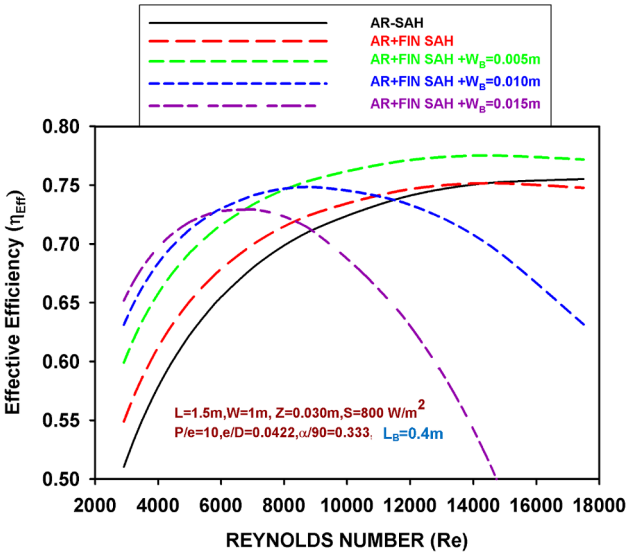

Fig. 8. Effect of Reynolds number and width of the baffle on effective efficiency of SAH when L_B = 0.4 m.

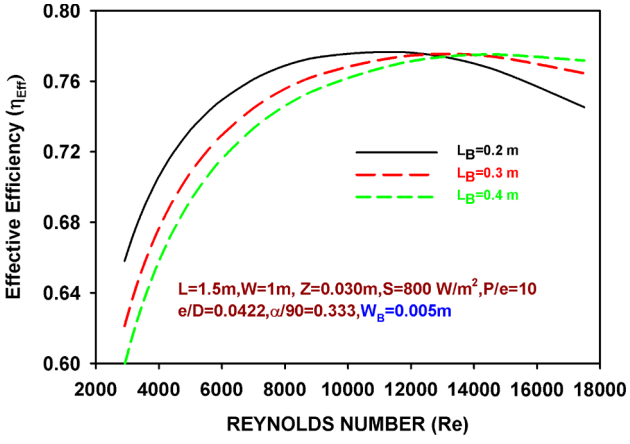

Fig. 9. Effect of Reynolds number and length of the baffle on effective efficiency of SAH.

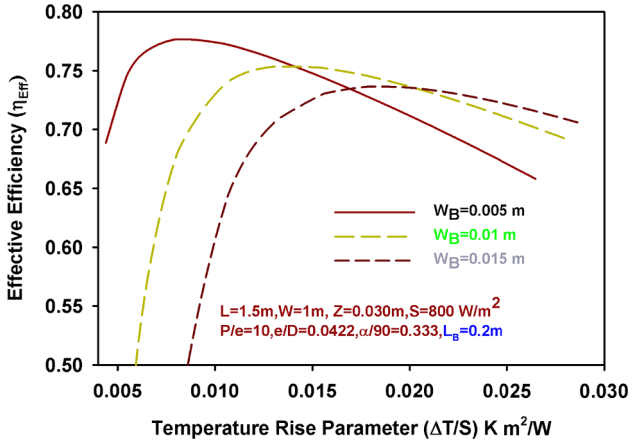

Fig. 10. Effective efficiency as a function of Temperature rise parameter and width of the baffle.

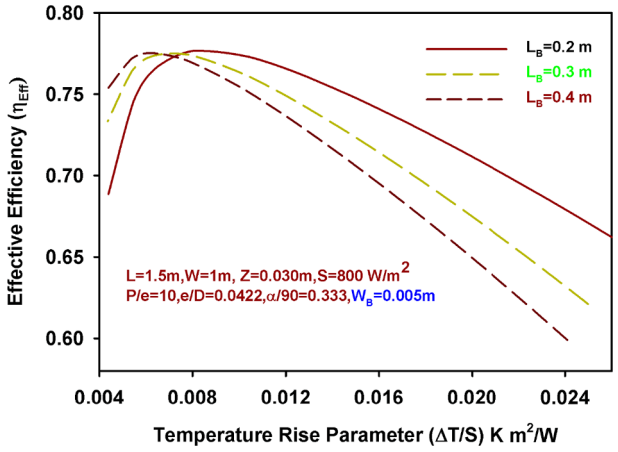

Fig. 11. Effective efficiency as a function of temperature rise parameter and length of the baffle.

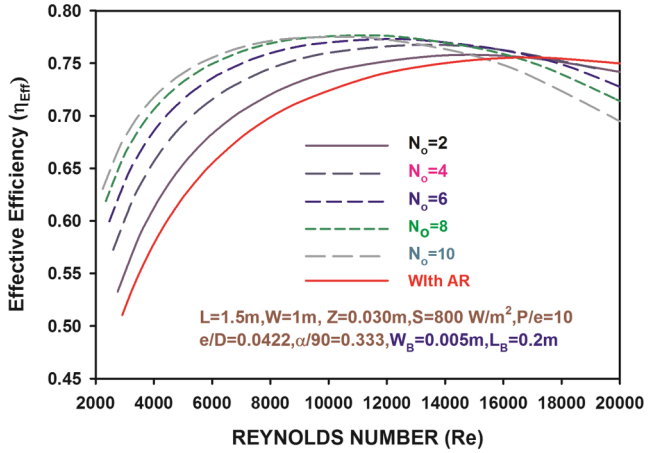

Fig. 12. Effective efficiency as a function of Reynolds Number and number of fins.

radiation increases from 400 W/m^2 to 800 W/m^2, an appreciable increment in effective efficiency is observed. Beyond this value, there is no further improvement. Therefore, it is concluded that the proposed solar air heater performs better at the solar intensity of 800 W/m^2.

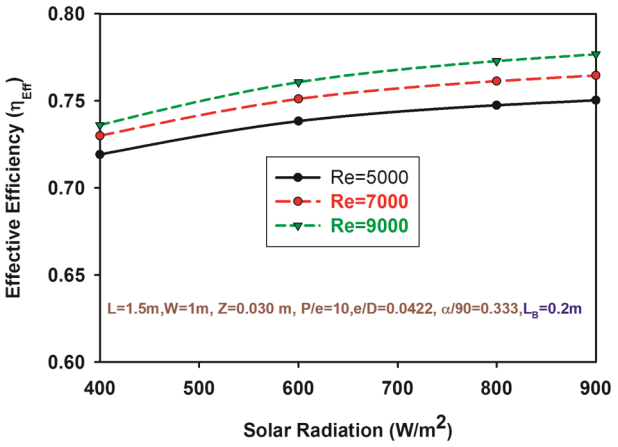

Fig. 13. Effective efficiency as a function of solar radiation for various Reynolds number.

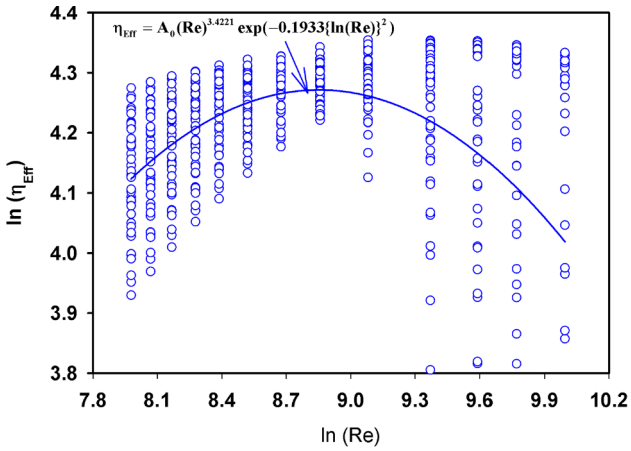

Fig. 14. Plot of ln(η_{Eff}) as a function of ln (*Re*) for all the values of analytical results.

4.5. Development of correlation

The statistical correlation is developed to predict the effective efficiency of the proposed SAH configuration as a function of non-dimensional parameters such as baffle length ratio (L_B/L) baffle width ratio (W_B/W), number of fins (N_o) and Reynolds number (*Re*). For the developing this correlation, the effective efficiency is plotted in terms of logarithmic scale against the *Re* in logarithmic scale as shown in Fig. 14. Using the regression analysis, the nonlinear relationship between effective efficiency and *Re* is represented by the equation as

$$\eta_{Eff} = A_0(Re)^{3.4221}\exp(-0.1933\{\ln(Re)\}^2) \quad (46)$$

In the above equation, A_0 represents the functional parameter of and $\ln N_O$.

From the regression analysis, the mathematical relationship can be expressed as

$$\eta_{Eff} = D_0(Re)^{3.4221}\exp(-0.1933\{\ln(Re)\}^2)\left(\frac{W_B}{W}\right)^{-0.3316}\exp\left(-0.0254\left\{\ln\left(\frac{W_B}{W}\right)\right\}^2\right)\left(\frac{L_B}{L}\right)^{0.1328}\exp\left(0.05\left\{\ln\left(\frac{L_B}{L}\right)\right\}^2\right)(N_o)^{0.1137}\exp(-0.0242\{\ln(N_o)\}^2) \quad (49)$$

Final correlation found out for effective efficiency as function of various design and operating parameters in the range of *Re* 2800–14,000, w_B of 0.005–0.015 m, L_B of 0.2–0.4 m and number of fins N_o of 2–10 is given by

$$\eta_{Eff} = 6.76\times10^{-6}(Re)^{3.4221}\exp(-0.1933\{\ln(Re)\}^2)\left(\frac{W_B}{W}\right)^{-0.3316}\exp\left(-0.0254\left\{\ln\left(\frac{W_B}{W}\right)\right\}^2\right)\left(\frac{L_B}{L}\right)^{0.1328}\exp\left(0.05\left\{\ln\left(\frac{L_B}{L}\right)\right\}^2\right)(N_o)^{0.1137}\exp(-0.0242\{\ln(N_o)\}^2) \quad (50)$$

This correlation can be used for predicting the effective efficiency with maximum deviation of ± 13% as shown in Fig. 18 of parity plot.

width ratio. Now the relationship between the terms $\left[\frac{\eta_{Eff}}{(Re)^{3.4221}\exp(-0.1933\{\ln(Re)\}^2)}\right]$ and $\ln\frac{W_B}{W}$ is shown in Fig. 15. From the regression analysis, the mathematical relationship is expressed as

$$\eta_{Eff} = B_0(Re)^{3.4221}\exp(-0.1933\{\ln(Re)\}^2)\left(\frac{W_B}{W}\right)^{-0.3316}\exp\left(-0.0254\left\{\ln\left(\frac{W_B}{W}\right)\right\}^2\right) \quad (47)$$

Similarly, the coefficient B_0 in the above equation is the function of other design parameters. Fig. 16 shows the significance of length ratio on effective efficiency in the log to log scale for the parameters $\frac{\eta_{Eff}}{(Re)^{3.4221}\exp(-0.1933\{\ln(Re)\}^2)\left(\frac{W_B}{W}\right)^{-0.3316}\exp\left(-0.0254\left\{\ln\left(\frac{W_B}{W}\right)\right\}^2\right)}$ and $\ln\frac{L_B}{L}$. The relationship between the parameters is written as

$$\eta_{Eff} = C_0(Re)^{3.4221}\exp(-0.1933\{\ln(Re)\}^2)\left(\frac{W_B}{W}\right)^{-0.3316}\exp\left(-0.0254\left\{\ln\left(\frac{W_B}{W}\right)\right\}^2\right)\left(\frac{L_B}{L}\right)^{0.1328}\exp\left(0.05\left\{\ln\left(\frac{L_B}{L}\right)\right\}^2\right) \quad (48)$$

In Eq. (48), C_o is the function of other design parameters. Fig. 17 illustrates the relationship between

$$\left[\frac{\eta_{Eff}}{(Re)^{3.4221}\exp(-0.1933\{\ln(Re)\}^2)\left(\frac{W_B}{W}\right)^{-0.3316}\exp\left(-0.0254\left\{\ln\left(\frac{W_B}{W}\right)\right\}^2\right)\left(\frac{L_B}{L}\right)^{0.1328}\exp\left(0.05\left\{\ln\left(\frac{L_B}{L}\right)\right\}^2\right)}\right]$$

4.6. Comparison with literature data

Fig. 19 compares the effective efficiency of the present work with literature data. In this figure, the proposed SAH shows the evidence of higher effective efficiency compared with existing model. The effective efficiency of proposed SAH is enhanced by 23.1% and 15.5% compared with work reported in the literature (Mohammadi and Sabzpooshani, 2013, 2014). It is due to fact that the artificial roughness breaks the laminar sub layer leading to flow separation thereby improving the reattachment points. In addition with, fins with baffles enhance the heat transfer rate by increasing the turbulence and heat transfer area.

5. Conclusions

The mathematical model is developed for analyzing the modified solar air heater with artificially roughened absorber plate integrated

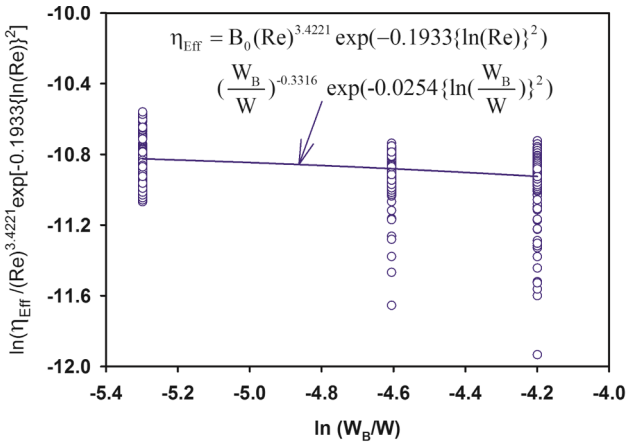

Fig. 15. Plot of $\ln\left[\frac{\eta_{Eff}}{(Re)^{3.4221}\exp(-0.1933\{\ln(Re)\}^2)}\right]$ as a function of $\ln\left[\frac{w_B}{W}\right]$

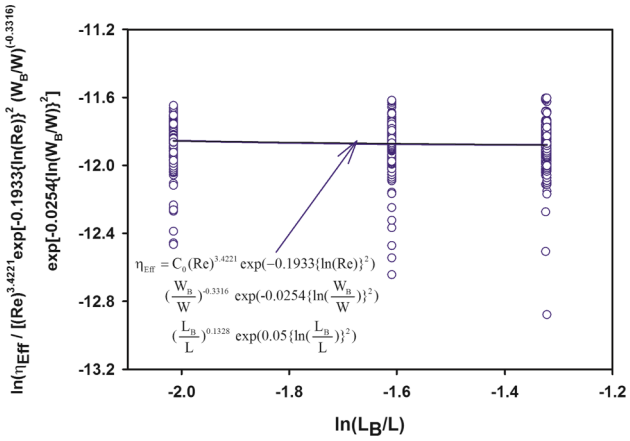

Fig. 16. Plot of

$$\frac{\eta_{Eff}}{(Re)^{3.4221}\exp(-0.1933\{\ln(Re)\}^2)\left(\frac{w_b}{W}\right)^{-0.3316}\exp\left(-0.0254\left\{\ln\left(\frac{w_b}{W}\right)\right\}^2\right)}$$ as a function of $\ln\left[\frac{L_B}{L}\right]$

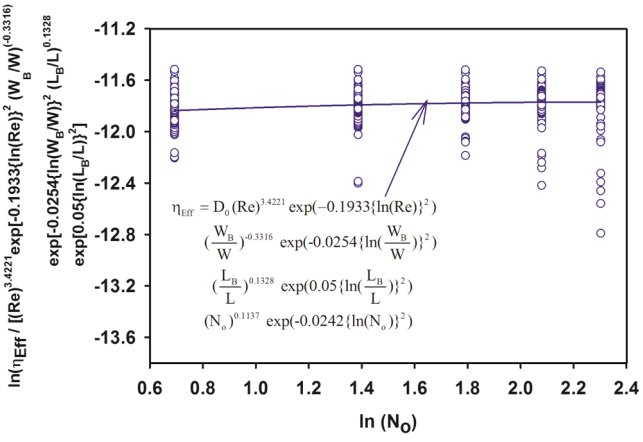

Fig. 17. Plot of

$$\left[\frac{\eta_{Eff}}{(Re)^{3.4221}\exp(-0.1933\{\ln(Re)\}^2)\left(\frac{w_b}{W}\right)^{-0.3316}\exp\left(-0.0254\left\{\ln\left(\frac{w_b}{W}\right)\right\}^2\right)\left(\frac{L_b}{L}\right)^{0.1328}\exp\left(0.05\left\{\ln\left(\frac{L_b}{L}\right)\right\}^2\right)}\right]$$

as a function of ln [N_o]

fins with baffles. From the analysis, the thermal, effective efficiencies, temperature rise parameters are evaluated and the following significant conclusions are drawn.

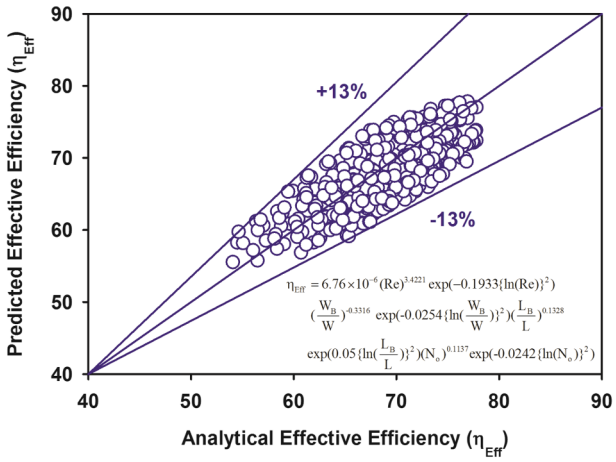

Fig. 18. Comparison between analytical and predicted values

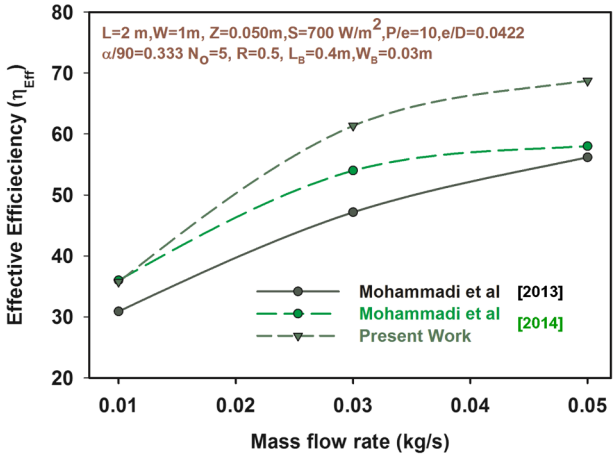

Fig. 19. Comparison between present and previous works based on effective efficiency

- Based on the thermal efficiency values of configured SAH, it is concluded that SAH with arc shaped rib roughened absorber plate integrated fins with baffles have better performance compared with other two models.
- The maximum thermal efficiency of the proposed SAH is 81.9% and it is also observed that the maximum enhancement in thermal efficiency is 28.3% compared with arc shaped rib roughened SAH at W_B = 0.015 m and L_B = 0.2 m. From the above discussions, it is concluded that increasing the baffle width and decreasing the length of the baffles improve the thermal efficiency.
- With respect to effective efficiency, it is observed that artificially roughened absorber plate integrated fins with baffled SAH enhances the performance by 27.1% compared with arc shaped rib roughened SAH at W_B = 0.005 m and L_B = 0.2 m.
- The effective efficiency of the proposed SAH follows a declining trend at higher mass flow rate conditions and when the W_B greater than 0.005 m
- At lower mass flow rates, increasing the number fins improves the effective efficiency and at higher mass flow rates it reverses the trend due to higher pressure drop.
- Finally, the correlation for predicting the effective efficiency of the proposed SAH is derived as a function of Reynolds number, baffle width and length ratios, and number of fins.

References

Ammari, H.D., 2003. A mathematical model of thermal performance of a solar air heater

with slats. Renew. Energy 28, 1597–1615.
Bahrehmand, D., Ameri, M., Gholampour, M., 2015. Energy and exergy analysis of different solar air collector systems with forced convection. Renew. Energy 83, 1119–1130.
Bhushan, B., Singh, R., 2012. Thermal and thermohydraulic performance of roughened solar air heater having protruded absorber plate. Sol. Energy 86, 3388–3396.
Chamoli, S., Thakur, N.S., 2016. Correlations for solar air heater duct with V-shaped perforated baffles as roughness elements on absorber plate. Int. J. Sustain. Energy 35, 1–20.
Chand, S., Chand, P., 2018. Parametric study on the performance of solar air heater equipped with louvered fins. J. Mech. Sci. Technol. 32, 3965–3973.
Chauhan, R., Thakur, N.S., 2014. Investigation of the thermohydraulic performance of impinging jet solar air heater. Energy 68, 255–261.
Duffie, J.A., Beckman, W.A., 2013. Solar Engineering of Thermal Processes, fourth ed. .
Fakoor Pakdaman, M., Lashkari, A., Basirat Tabrizi, H., Hosseini, R., 2011. Performance evaluation of a natural-convection solar air-heater with a rectangular-finned absorber plate. Energy Convers. Manage. 52, 1215–1225.
Fudholi, A., Sopian, K., Ruslan, M.H., Othman, M.Y., 2013. Performance and cost benefits analysis of double-pass solar collector with and without fins. Energy Convers. Manage. 76, 8–19.
Hollands, K.G.T., Unny, T.E., Raithby, G.D., Konicek, L., 1976. Free convective heat transfer across inclined air layers. J. Heat Transfer 98, 189.
Ong, K.S., 1995. Thermal performance of solar air heaters: mathematical model and solution procedure. Sol. Energy 55, 93–109.
Karim, M.A., Hawlader, M.N.A., 2006. Performance investigation of flat plate, v-corrugated and finned air collectors. Energy 31, 452–470.
Karmare, S.V., Tikekar, A.N., 2007. Heat transfer and friction factor correlation for artificially roughened duct with metal grit ribs. Int. J. Heat Mass Transf. 50, 4342–4351.
Karwa, R., Chauhan, K., 2009. Performance evaluation of solar air heaters having v-down discrete rib roughness on the absorber plate. Energy 35, 398–409.
Kumar, K., Prajapati, D.R., Samir, S., 2017. Heat transfer and friction factor correlations development for solar air heater duct artificially roughened with 'S' shape ribs. Exp. Therm. Fluid Sci. 82, 249–261.
Kumar, R., Chand, P., 2018. Performance prediction of extended surface absorber solar air collector with twisted tape inserts. Sol. Energy 169, 40–48.
Kumar, R., Chand, P., 2017. Performance enhancement of solar air heater using herringbone corrugated fins. Energy 127, 271–279.
Matheswaran, M.M., Arjunan, T.V., Somasundaram, D., 2018a. Analytical investigation of solar air heater with jet impingement using energy and exergy analysis. Sol. Energy 161, 25–37.
Matheswaran, M.M., Arjunan, T.V., Somasundaram, D., 2018b. Energetic, exergetic and enviro-economic analysis of parallel pass jet plate solar air heater with artificial roughness. J. Therm. Anal. Calorim. https://doi.org/10.1007/s10973-018-7727-4.
Matheswaran, M.M., Arjunan, T.V., Somasundaram, D., 2018c. Analytical investigation of exergetic performance on jet impingement solar air heater with multiple arc protrusion obstacles. J. Therm. Anal. Calorim. https://doi.org/10.1007/s10973-018-7926-z.
Mohammadi, K., Sabzpooshani, M., 2014. Appraising the performance of a baffled solar air heater with external recycle. Energy Convers. Manage. 88, 239–250.
Mohammadi, K., Sabzpooshani, M., 2013. Comprehensive performance evaluation and parametric studies of single pass solar air heater with fins and baffles attached over the absorber plate. Energy 57, 741–750.
Priyam, A., Chand, P., 2018. Effect of wavelength and amplitude on the performance of wavy finned absorber solar air heater. Renew. Energy 119, 690–702.
Priyam, A., Chand, P., 2016. Thermal and thermohydraulic performance of wavy finned absorber solar air heater. Sol. Energy 130, 250–259.
Rai, S., Chand, P., Sharma, S.P., 2018. Evaluation of thermo hydraulic effect on offset finned absorber solar air heater. Renew. Energy 125, 39–54.
Rai, S., Chand, P., Sharma, S.P., 2017. An analytical investigations on thermal and thermohydraulic performance of offset finned absorber solar air heater. Sol. Energy 153, 25–40.
Sahu, M.K., Prasad, R.K., 2017. Thermohydraulic performance analysis of an arc shape wire roughened solar air heater. Renew. Energy 108, 598–614.
Singh, S., Dhiman, P., 2015. Thermal performance analysis of a rectangular longitudinal finned solar air heater with semicircular absorber plate. J. Sol. Energy Eng. 138.
Varun, Saini, R.P., Singal, S.K., 2008. Investigation of thermal performance of solar air heater having roughness elements as a combination of inclined and transverse ribs on the absorber plate. Renew. Energy 33, 1398–1405.
Yadav, S., Kaushal, M., Siddhartha, Varun, 2013. Nusselt number and friction factor correlations for solar air heater duct having protrusions as roughness elements on absorber plate. Exp. Therm. Fluid Sci. 44, 34–41.
Yeh, H.M., Ho, C.D., Lin, C.Y., 2000. Effect of collector aspect ratio on the collector efficiency of upward type baffled solar air heaters. Energy Convers. Manage. 41, 971–981.